Palaeogeography, Palaeoclimatology, Palaeoecology 479 (2017) 61–70

Contents lists available at ScienceDirect

Palaeogeography, Palaeoclimatology, Palaeoecology

journal homepage: www.elsevier.com/locate/palaeo

Sediment provenance variations in the southern Okhotsk Sea over the last 180 ka: Evidence from light and heavy minerals

Kun-Shan Wang [a,b], Xue-Fa Shi [a,b,*], Jian-Jun Zou [a,b], Selvaraj Kandasamy [c], Xun Gong [d], Yong-Hua Wu [a,b], Quan-Shu Yan [a,b]

[a] Key Laboratory of Marine Sedimentology and Environmental Geology, First Institute of Oceanography, SOA, Qingdao 266061, China
[b] Laboratory for Marine Geology, Qingdao National Laboratory for Marine Science and Technology, Qingdao, 266061, China
[c] Department of Geological Oceanography and State Key Laboratory of Marine Environmental Science, Xiamen University, Xiamen 361005, China
[d] Alfred-Wegener-Institut Helmholtz-Zentrum für Polar- und Meeresforschung, Am AltenHafen 26, 27568 Bremerhaven, Germany

ARTICLE INFO

Article history:
Received 25 August 2016
Received in revised form 31 March 2017
Accepted 9 April 2017
Available online 27 April 2017

Keywords:
Light and heavy minerals
Volcanic detrital
Sediment provenance
Sea ice
Okhotsk Sea

ABSTRACT

In this study, we investigate light and heavy minerals in sediment core OS03-1 located at the Academy of Sciences Rise of the southern Okhotsk Sea to determine their distributions and sources over the last 180 ka (thousand years). The sediment mainly consists of terrigenous and volcanic detritus. Ubiquitous drop-stones and volcanic detritus throughout the core and high detrital input suggest that sea ice, driven by wind and Kamchatka Current, was the main transport agent of detrital materials to the southern Okhotsk Sea. The ternary diagram of heavy minerals (hornblende-hypersthene-epidote) shows an expansion of detritus provenance from the eastern in cold periods to the northeastern in warm intervals of the Okhotsk Sea. It mainly relates to the shift of Aleutian Low. Combined with previous records, accumulation rates of quartz indicated a maximum extent but not perennial sea ice coverage during the glacial periods.

1. Introduction

Sea ice is a key element of the climate system, which is not only unilaterally forced by oceanic and atmospheric conditions, but also participates in a variety of feedback effects (Untersteiner, 1986). The Okhotsk Sea, the northernmost boundary of permanent seasonal sea ice cover in the north Pacific, plays an important role in the regional and global climate, such as ventilating the intermediate water in the North Pacific. Based on various proxy evidences such as ice rafted-debris (IRD) (Liu et al., 2006; Nürnberg et al., 2011; Nürnberg and Tiedemann, 2004; Sakamoto et al., 2005; Sakamoto et al., 2006), microfossils (Gorbarenko et al., 2002; Itaki and Ikehara, 2004; Katsuki et al., 2010; Khusid et al., 2005; Okazaki et al., 2003a, 2003b; Shiga and Koizumi, 2000) and sea surface temperatures (SST) (Harada et al., 2008), these studies revealed that sea ice extent has varied in the Okhotsk Sea. For example, an extended but not perennial sea ice cover was present over a great part of the sea during the Last Glacial Maximum (LGM) (Shiga and Koizumi, 2000; Wang and Wang, 2008). Sakamoto et al. (2005) reported thirteen climatic intervals of enhanced sea ice cover during the last 100 ka and postulated that the provenance of IRD to the Okhotsk Sea was mostly from the adjacent lands. Using detrital minerals and planktonic foraminifera $\delta^{18}O$, Nürnberg et al. (2011)further suggested that the significant contribution of IRD from the Kamchatka Iceberg occurred in Marine Isotope Stage (MIS) 6 and 3. Based on the abundances of radiolarian and diatom species, a mechanism controlling the variation in sea ice cover by the position of Aleutian Low (AL) has been proposed (Itaki and Ikehara, 2004; Katsuki et al., 2010). Zou et al. (2015) found that the expanded sea ice cover occurred in MIS 5.3 was closely related to the Siberian High Index (Li and Liu, 2012). However, the IRD transport and the corresponding variations in sea ice cover in the southern Okhotsk Sea are still unclear due to the scarcity of direct indicator of paleosea-ice cover.

Sea ice incorporates sediment either by suspension freezing where ice crystals form near the sea floor and float the sediment to the surface or by anchor ice that forms on the sea floor and when thick enough to become buoyant, it lifts the sediment off the bottom incorporated into the ice and floats it to the surface. Fast ice can also form on the shoreline and be floated by waves or tides. The ice acts as a raft, providing buoyancy to any debris included within it or on its surface. The sea ice melts and fragments during its drift. As it melt, at a rate dependent on the temperature of the water, and its size and velocity, any included sediment is released, results the deposition of IRD (Nürnberg et al., 1994; Dowdeswell, 2009). In general, the IRD carried by the terrigenous fraction is an assorted mixture of gravel, sand, silt and clay size materials (Gorbarenko et al., 2002). However, the defined clastic diameter of terrigenous materials considered as IRD is dominantly of sand size

* Corresponding author at: Key Laboratory of Marine Sedimentology and Environmental Geology, First Institute of Oceanography, SOA, Qingdao 266061, China.
E-mail address: xfshi@fio.org.cn (X.-F. Shi).

http://dx.doi.org/10.1016/j.palaeo.2017.04.017
0031-0182/

between 63 μm and 2000 μm (Bigg et al., 2008; Gorbarenko et al., 2008; Malakhov et al., 2009), whereas that for drop-stones should be larger than sand, i.e. >2000 μm (Sakamoto et al., 2005; Selvaraj et al., 2012). Although the range of IRD often varies based on the purpose of research problem addressed and the area of study, the minimum grain size limit of IRD for mineralogical studies is 63 μm (Carter et al., 2002; John and Krissek, 1999). Geochemical and mineralogical analyses of IRD can be ideal to reconstruct the source of iceberg sand the transport pathways (Bischof et al., 1996; Small et al., 2013). Studies on the distribution of detrital minerals have mainly focused on the mineral composition of volcanic ash, whereas studies on rock-forming minerals in surface and core sediments in the Okhotsk Sea are scarce (Derkachev and Nikolaeva, 2007; Nicholson et al., 2014; Wang et al., 2014).

In this study, we examine the mineral compositions and weight contents of IRD with a diameter between 63 and 125 μm, the lithology of drop-stones and the grain size in the late Quaternary sediment records from the Academy of Science Rise in the southern Okhotsk Sea. Based on the comparison with the heavy mineral compositions of surface sediments in the Okhotsk Sea, we discuss the drift directions of sea ice and the provenance of IRD over the past 180 ka.

2. Oceanographic settings

The Okhotsk Sea is surrounded by Eurasian landmass in the north, North Pacific proper in the south, Sakhalin Island in the southwest and Kamchatka Island Arc in the northeast (Fig. 1). At present, typical characteristics for the Okhotsk Sea are counter-clockwise surface circulation, southernmost seasonal sea ice coverage, high primary productivity and formation of North Pacific Intermediate Water (NPIW). The surface circulation in the Okhotsk Sea is composed by northward West Kamchatka Current and southward East Sakhalin Current, which is a part of the subarctic circulation system in the North Pacific (Takahashi, 1998). The southernmost extension of modern sea ice reaches 43° N; hence, the Okhotsk Sea is regarded as a relic of the glacial period (Okazaki et al., 2003a, 2003b). The formation and melting of sea ice have not only greatly affect the surface hydrology and the vertical structure of water mass, but also affects primary productivity and depositions in the Okhotsk Sea.

Major factors for Okhotsk sea ice formation are the freshwater input from the Amur River and the strong Siberian winter wind from the west to the northwest (Okazaki et al., 2005; Shiga and Koizumi, 2000). The latter is related to interaction between the Siberian High and the Aleutian Low (Martin et al., 1998). The southward drift of sea ice is mainly due to wind and ocean currents. The contribution of wind is typically greater than that of the ocean current (Simizu et al., 2014). Sea ice generally begins to build-up in November and greatest thickness of sea ice reaches approximately 1 m and up to 1.8 m in some areas in March. By the start of June, the majority of the sea ice has melted and the sea is free of ice from July to October. A study of sea ice dynamics using satellite imageries clearly revealed changes in the expansion and retreat of sea ice in the Okhotsk Sea (Cavalieri and Parkinson, 1987). The largest range of modern sea ice expansion has reached the southeastern part of the Okhotsk Sea, near the Kuril Basin (Minervin et al., 2015). The expansion and retreat of modern sea ice are considerably affected by wind and temperature (Kimura and Wakatsuchi, 1999). Under the effect of wind and currents, sea ice drifts from the north to the southeast. The formation, diffusion and ablation of sea ice can change ocean salinity, which in turn affects the formation of the Okhotsk Sea intermediate water.

3. Materials and methods

For the present investigation, we collected a 381-cm long sediment core OS03-1 (150°00′36″ E, 49°29′51″ N) from the Academy of Sciences Rise, located on the continental slope of the northern edge of the Kuril Basin (Fig. 1). The core was raised from water depths of ~1000 m using a gravity corer available on board R/V *Xuelong* during the Chinese Arctic Research Expedition. Because the annual sea ice cover extends to the core location (Yang and Honjo, 1996), we believe that core OS03-1 is ideal for the investigation of sea ice dynamics-related provenance changes of detrital delivery to the study area in the past.

The core was subsampled at 2 cm interval and all subsamples were measured for the content of different grain size fractions. The fraction of >40 μm was separated from bulk sediment sample via wet sieving and then was subjected to sonic shaking after drying at 60 °C. Subsequently, the fraction of >40 μm in each subsample was subdivided

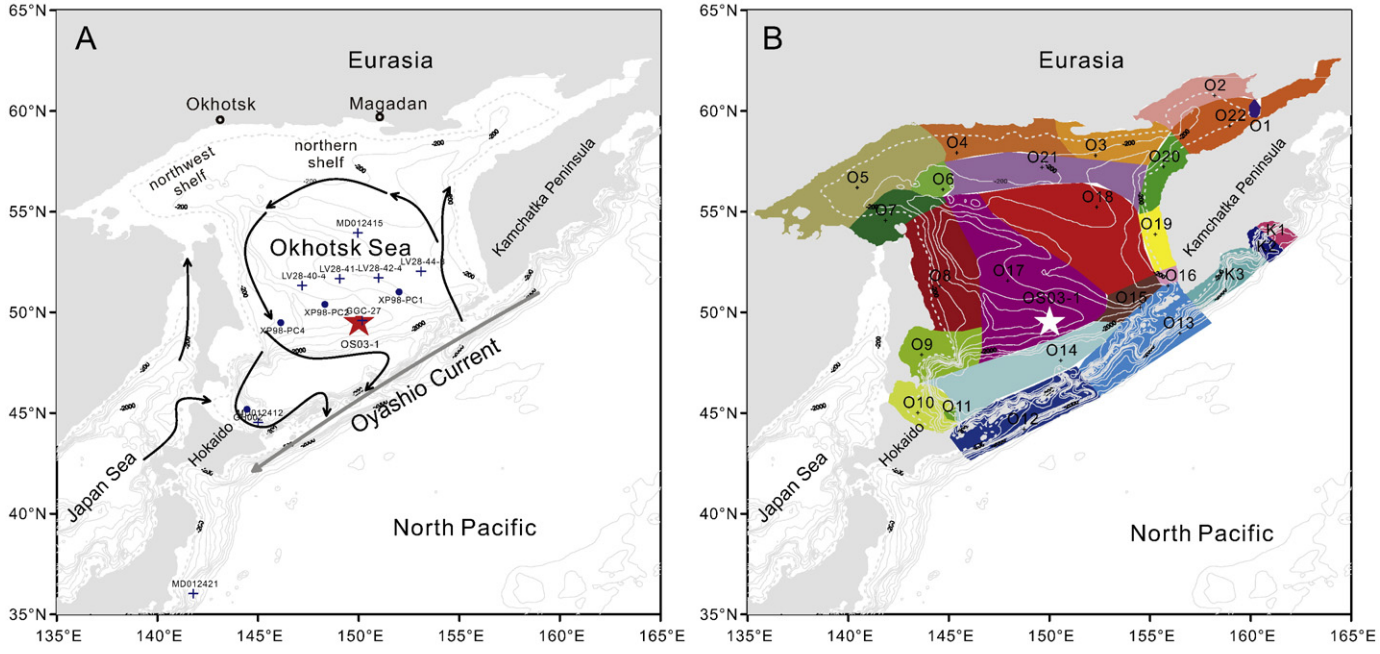

Fig. 1. A) Map showing the location of core OS03-1 (★) and the symbol "+" represents the locations of other cores mentioned in the text. The pattern of surface currents derives from Qiu (2001). The regions of northwest shelf and northern shelf cites from Martin et al. (1998). B) The distribution of hornblende and hypersthene ratios in the provinces of heavy minerals. (Modified from Derkachev and Nikolaeva (2007) that cited from Petelin (1957)).

into four sub-fractions, namely 40–63 μm (coarse silt), 63–125 μm (fine sand), 125–2000 μm (fine sand to coarse sand) and 2–10 mm (granules). The content of >2 mm material was not included in weight calculations in order to avoid misleading peak values caused by the sporadic occurrence of individual granules.

The light and heavy minerals were analysed in the very fine sand fraction (63–125 μm). This fraction of sands was wet-sieved by a nylon mesh and light and heavy minerals were separated using bromoform with specific gravity of 2.89 g/cm^3. We identified over 300 grains in each subsample and then counted using a binocular microscope. Based on the percentage of each mineral type as well as the data of bulk sediment dry weight, 63–125 μm class weight, mineral density and the weight content of each mineral were calculated. The flux of coarse fraction and detrital minerals are expressed by mass accumulation rate (MAR), which was calculated by multiplying the linear sedimentation rate (LSR) by the dry bulk density (DBD) (MAR = LSR × DBD) using a similar method adopted by Nürnberg et al. (2011).

Age model establishments for core OS03-1 are reported by Zou et al. (2015) based on oxygen isotope data and accelerator mass spectrometry (AMS) ^{14}C. Briefly, reference ages were determined on one ^{14}C dating of *Neogloboquadrina pachyderma* (sinistral) by accelerator mass spectrometry at a depth of 16–18 cm and δ^{18}O stratigraphy of benthic foraminifera (*Uvigerina* spp.). The bottom of core OS03-1 was estimated to be about 180 ka with a resolution of ~950 years/sample.

4. Results

4.1. Lithology and grain size variation

We divided the core OS03-1 into two lithologic units from the top to bottom. Unit 1 in the upper 0–9 cm (<~5 ka) of the core contains dark ooze. This unit is extremely soft and has high-water content with hydrogen sulphide odour. Consistent with this observation, the degree of gray of sediment color in the L* values in this unit decreased sharply and in the b* values showed lower (Fig. 2). Unit 2 (9–381 cm) contains dark-gray and green–gray sediments and is dominated by sandy silt and silty sand with abundant drop-stones of various sizes. The core has three distinct volcanic ash layers, reported by Zou et al. (2015). Both L* and b* values simultaneously sharply decreased at three volcanic layers (Fig. 2).

The weight % of very fine sand (63–125 μm) is higher than coarse silt in average values in core OS03-1 with a mean content of 12.5%. Peak values of this fraction frequently seen in the MIS 6 (Fig. 2). The content of coarse silt (40–63 μm) is consistent in the entire core and always lower than the content of very fine sand, except in MIS5, wherein the contents of both are nearly the same. On the other hand, the content of medium to very coarse sand (125–2000 μm) is almost <10% throughout the core.

4.2. Distribution and petrological characteristics of drop-stones

Core OS03-1 contains a large number of drop-stones (>2 mm), with the largest diameter of 5 cm and the weight of 86 g (Table 1). The drop-stones distribution in the core is ubiquitous and most peak values occur in MIS 5 and MIS 3.3 (Fig. 2), but without forming any distinct drop-stones layer. The maximum number of drop-stones occurs at a depth interval of 244–246 cm (121.2–122.5 ka) with 27 grains. Among them, the main composition is pumice for 17 grains that measuring from 2 to 10 mm. The color of the most drop-stones is black-green, although some are gray–white and black in colors.

The majority of drop-stones have abrasive and smooth surfaces, and are spherical to sub-angular in shapes (Fig. 3). Petrologically, dropstones are dacite, andesite and rhyolite of intermediate and acid rocks. Dacites, basaltic andesite (Fig. 3) and vitric matrix andesite mainly occur at the upper part of the core, whereas andesite, biotite andesite and rhyolite occur at the lower part of the core. Dacite, a black, subangular to subrounded rock fragment with smooth surface and grooves occurs mainly in the upper part of the core (Table 1). Rocks have porphyritic texture, fine-grain texture and rhyolitic structure. Phenocrysts are mainly plagioclase and quartz. Andesite has many types, including basaltic andesite, vitric matrix andesite, biotite vitric matrix andesite and biotite pyroxene andesite, which are mainly distributed in the middle and lower parts of the core and has gray–white, black and gray–green colors. Rhyolite comprises the largest volume and weight of drop-stones in the core and it has a sub-rounded shape, showing gray–black in the body and gray–green to grayish–white in the fresh rock fracture (Fig. 3).

4.3. Light and heavy minerals

The mean content of light minerals in the core is 11.8%, with the highest reaching 34.86% (Fig. 4). The average weight content of heavy minerals is 0.47%, with the highest reaching 2.93%. Plagioclase and quartz dominate the category of light minerals, whereas hornblende,

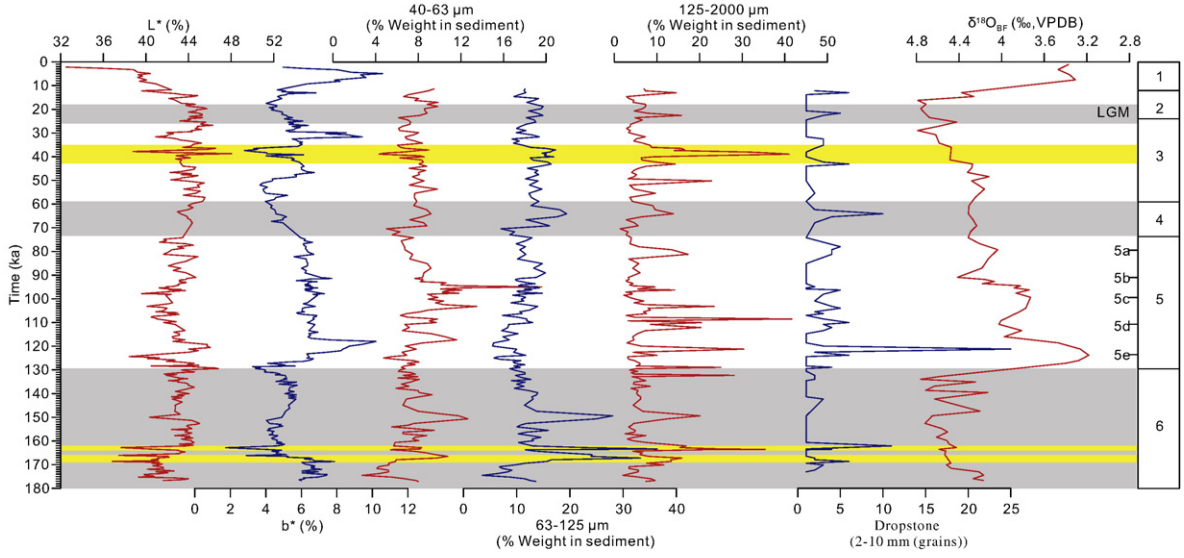

Fig. 2. Variations in sediment color (L*, b*), coarse fraction concentrations (wt%) and number of drop-stones in core OS03-1. Yellow bar indicates volcanic layers. Gray bar notes glacial periods.

Table 1
Petrological characteristics of drop-stones (>10 mm).

Number	Depth (cm)	Appearance	Texture, structure and mineral composition (rock thin section)	Rock types
1	4–6	Black color; smooth and subrounded; cracks, pits and scratches in surface; homogeneous.	Porphyritic texture, rhyolitic structure. Phenocryst of plagioclase, no dark minerals. Aphanitic groundmass	Dacite
2	45–46	Black color and slightly gray; slightly rough surface, see scratches; subangular to subrounded.	Fine phanerocrystalline texture; crystal main quartz, allotriomorhpic granular texture, a little plagioclase shows polysynthetic twin; biotite crystallic texture	Dacite
3	46–48	Black color, subangular, uneven surface, see feldspar crystal	Porphyritic texture, larger phenocrysts, main plagioclase being polysynthetic twin, others including hornblende, augite being lower level interference color.	Basaltic andesite (Fig. 3)
4	116–118	Gray color, slightly pale; clear angular, a little rounded; smooth surface, occasionally scratches; larger phenocrysts (quartz, feldspar).	Vitreous texture, being a little directional distribution; amygdaloidal structure; with the spherical magnetite crystallite in different sizes. Phanerocryst including brown bitotie being dark margin, plagioclase and hornblende.	Andesite (vitreous groundmass)
5	122–124	Gray white, porous, friction sensitivity, subangular to subrounded, obvious scratches; see larger transparent mineral crystals and black cinders	Vitrophyric texture, rhyolitic structure and vesicular structure; partial carbonation.	Pumice (vitreous groundmass)
6	122–124	Black color, in fracture being black gray. Fine granular structure, homogeneous, smooth surface being little scratched and pits, subangular to subrounded (edges are rounded)	Microlite texture; massive structure; plagioclase microlite as groundmass; no phenocrysts.	Andesite
7	146–148	Black color, smooth surface and more pits; homogeneous and being felsitic structure.	Porphyritic texture; biotite and pyroxene as phenocrysts have been weathered; see magnetite.	Biotite andesite
8	162–164	Gray white color; larger phenocryst may be feldspar, >0.5 mm; a greater black crystal, the composition is undetermined; the surface pits larger; subrounded.	Being vesicular structure and chloritization; normal and typical characteristics of andesite, plagioclase and hornblende as phenocrysts, magnetite appears much.	Andesite (Fig. 3)
9	182–184	Black with green color; subangular, uneven surface; homogeneous composition	Hyalopilitic texture; plagioclase, pyroxene and biotite as phenocrysts.	Biotite andesite
10	212–214	Gray white, subangular to subrounded; relatively smooth surface being pits, see minerals that amphibole and feldspar.	A phenocryst may be a rock detritas (possible diorite, with rhyolitic structure), the Phenocryst may be a xenolith, being eutectic margins.	andesite (glass groundmass) cemented diorite
11	242–244	Gray green, rounded; smooth surface; a little dark minerals; transparent minerals mainly composed of plagioclase and quartz.	Porphyritic texture; phenocryst for plagioclase and quartz; hornblende for sericitization; appeared pyroxene.	Diorite porphyrite (Fig. 3)
12	244–246	Gray green, slightly white tone; smooth surface, subrounded; homogeneous composition.	Vitreous texture; secondary alteration and radial; pyroxene illusion.	Andesite
13	309–311	The biggest one of drop-stones, gray black, fracture gray green; see quartz and feldspar crystals, dark minerals; subrounded, edges rounded.	Obvious felsitic texture; phenocryst for plagioclase and quartz.	Rhyolite (Fig. 3)
14	336–338	Black, subrounded, edges rounded, being pits in surface; a larger phenocryst.	Alteration; vitreous texture and porphyritic texture; vitrophyric structure, developed vesicular structure.	Andesite (altered)

hyperthene, epidote and augite are common heavy minerals in this size class.

In the light minerals, the contents of plagioclase and quartz vary between 0.5 and 20.7% and between 0.3 and 5.9%, show relatively high average values in glacial periods (MIS 6, 4 and 2), respectively, it is 8.107, 7.645 and 6.558%, 1.934, 3.341 and 3.275%. In the heavy minerals, the average content of common hornblende, augite and epidote is 0.051%, 0.03% and 0.067%, respectively and shows similar vertical patterns with those of quartz and plagioclase and exhibit minimum values in K2 ash layer (Fig. 4). However, quartz and plagioclase are extremely high in other two tephra layers (>5% and 20%, respectively) (Fig. 4), implying a mixture with terrigenous sediments. Similar phenomenon of occurrence of high contents of terrigenous detrital minerals in MR1 volcanic ash layer has been reported earlier (Derkachev et al., 2012). Hypersthene, an indicator of volcanic detritus, shows obvious peaks at volcanic layers (Fig. 4). Various volcanic glasses are widely distributed in the whole core with an increased content of brown volcanic glass during MIS 6 (Fig. 4).

5. Discussion

5.1. Transportations of coarse detrital materials

Since the location of core OS03-1 is close to the volcanic eruption area in the Kamchatka and Kuril Islands, the sediments are mostly terrigenous and volcanic in nature. Four dominant ways of terrigenous input to the Okhotsk Sea are: (i) suspended material transported from the surrounding land by Amur River; (ii) the coastal sediments from the northwest and north shelves through waves and sea ice; (iii) volcanic eruption from the Kuril Islands and the Kamchatka Peninsula (Nürnberg and Tiedemann, 2004); and (iv) the iceberg derived from the Kamchatka Peninsula (Nürnberg et al., 2011). The Amur River is the fourth largest river in Asia and the second largest river in Siberia (Ogi et al., 2001; Zhabin et al., 2010). However, after entering the Okhotsk Sea, the radiogenic isotopes (Sr and Nd) data shows that river-derived terrigenous materials mainly deposited along the western continental slope of the Okhotsk Sea (Yasuda et al., 2014) and the coarse grains could not pass through the deep Deryugin Basin (Nürnberg and Tiedemann, 2004). A study of rare earth elemental ratios of sediment core OS03-1, however, indicated that fine particles derived from Amur River could be transported to the southern Okhotsk Sea (Zou et al., 2015).

Detrital grains of light and heavy minerals observed under stereo and polarizing microscopes mostly exhibit sub-angular to sub-rounded shapes, with abrasive and uneven surfaces. The high content of unstable minerals (weak capability to resist weathering) suggests the characteristics of sea ice rafting of long-distance transport (Wang et al., 2014). The high accumulation rate of terrigenous biomarkers in core GGC-15, collected nearby our core (Fig. 1), also supports the fact that sea ice transport was the dominant mechanism of terrigenous materials transport to the southern Okhotsk Sea (Ternois et al., 2001). In addition, volcanic glasses/shards are widely distributed in the whole sediment core, indicating the significant contribution from the volcanic input. Except for three tephra layers observed in the analysed core, ubiquitous volcanic detritus suggests that sea ice might be the dominant way of transport of volcanic detritus. In addition, previous studies suggested that eolian input was a potential way of terrigenous input to the central Okhotsk Sea (Nürnberg and Tiedemann, 2004), but its contribution is

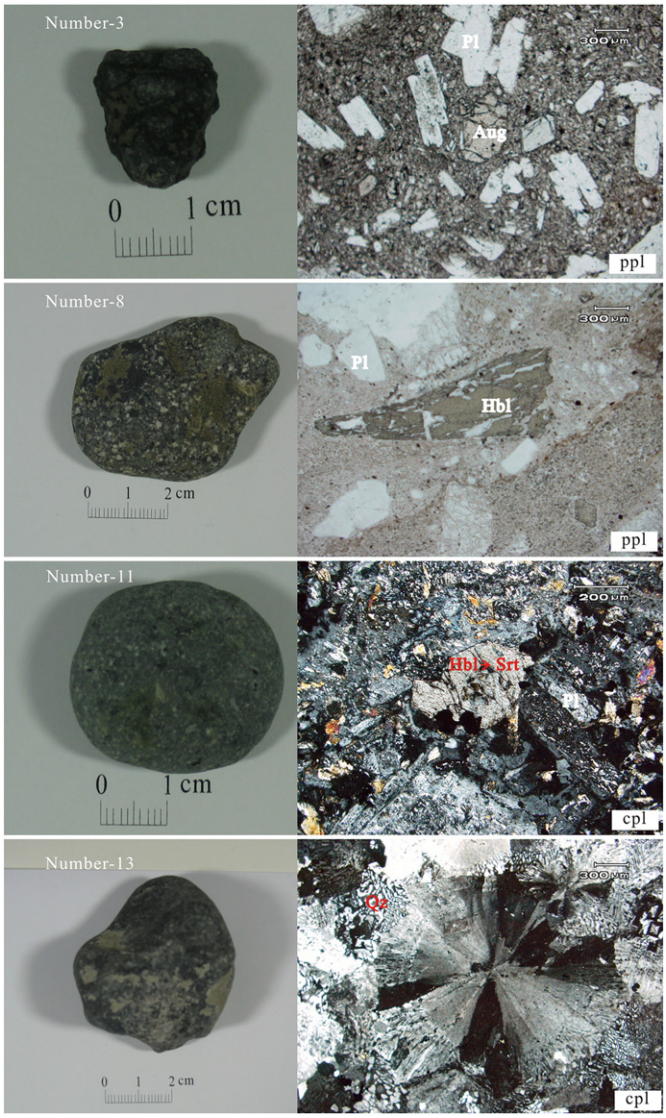

Fig. 3. Photographs of typical drop-stones (>10 mm) illustrating their shapes and petrographic images and their dominant mineralogy. Pl = plagioclase, Aug = augite, Hbl = hornblende, Srt = sericite, Qz = quartz, ppl = plane-polarizedlight, cpl = cross-polarized light.

very low compared to terrigenous and sea ice sources and therefore likely to be insignificant.

5.2. Provenance of coarse detrital material

The dominant minerals in core OS03-1 are quartz and plagioclase, which are consistent with other mineralogical and geochemical records available from cores MD01-2414 (Liu et al., 2006), OS03-1 (Zou et al., 2015) and LV28-42-4 & LV28-44-3 (Nürnberg et al., 2011). Core sediments investigated from the eastern part of Okhotsk Sea contain higher content of hornblende compared to cores from the western part of Okhotsk Sea and was deemed as derived from the Kamchatka Peninsula (Nürnberg et al., 2011; Sakamoto et al., 2005), while in the western Okhotsk Sea (PC4) the IRD was mainly supplied from the northern and the western continental margins (Sakamoto et al., 2005). However, the main hornblende source in the Okhotsk Sea is not from the Kamchatka Peninsula. A study of heavy minerals in surface sediments of the Okhotsk Sea indicated different heavy mineral provinces with various contents of common hornblende, hypersthene, epidote and garnet (Derkachev and Nikolaeva, 2007 (cited from Petelin, 1957)). Nicholson et al. (2014) reported that the common hornblende is a characteristic mineral in the sediments of northern coastline of the Okhotsk Sea and the eastern sea area of the Sakhalin, where the content of common hornblende is extremely high. In fact, the content of common hornblende is low in the sediments near the Kamchatka Peninsula and the Kuril Islands (Derkachev and Nikolaeva, 2007; Tikhomirov et al., 2012), while hypersthene is relatively higher in these areas (Tikhomirov et al., 2012). Hypersthene, magnetite and volcanic glass are higher in volcanic ash layers but lower in terrigenous sediment units and are also widely distributed in the core. A combination of these minerals indicates the degree of mixing of volcanic ash and IRD deposits as well as the sources of sea ice. As stated above, the provenances of common hornblende and hypersthene are significantly different from each other and therefore we can use the ratio of hornblende/hypersthene to discriminate the relative contribution between terrigenous and volcanic sources.

We compared the composition of heavy mineral grains with published data from surface sediments in the Okhotsk Sea to discriminate the detrital provenance. Based on the ratio of common hornblende to hypersthenes in surface sediments, Derkachev and Nikolaeva (2007) have divided the Okhotsk Sea into 19 mineral provinces (Fig. 1). Ternary diagrams of hornblende - epidote - hypersthene for core OS03-1 constructed to understand the sources of sediments show that the coarse fraction in core OS03-1 mainly sourced from areas around west and east Kamchatka Peninsula and Kuril Islands (Figs. 1 and 5), suggesting

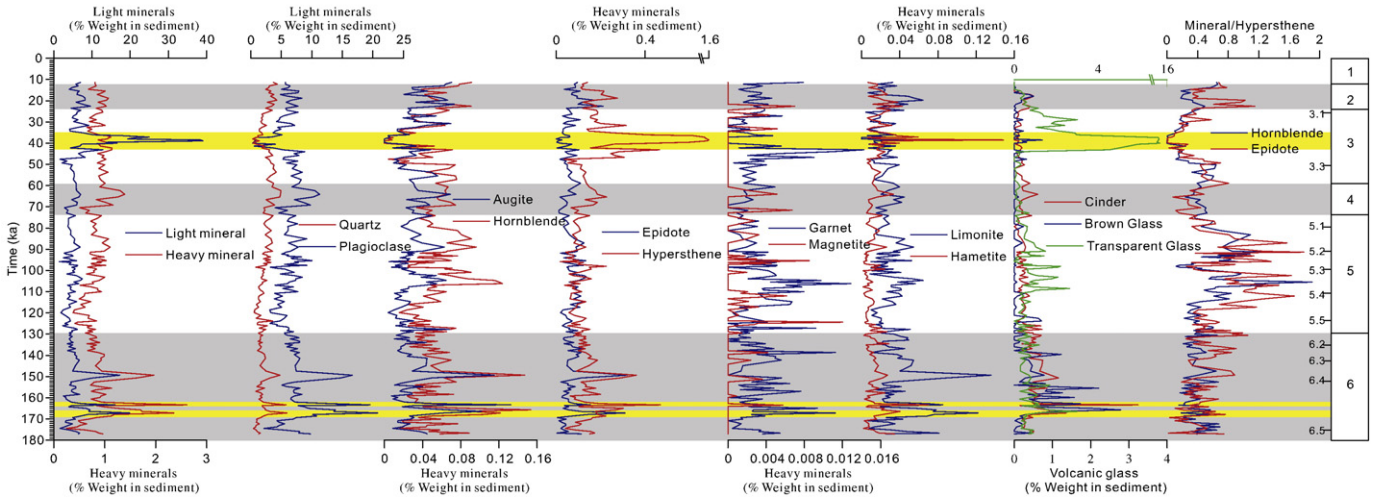

Fig. 4. Age versus contents of light and heavy minerals and volcanic glasses in core OS03-1.

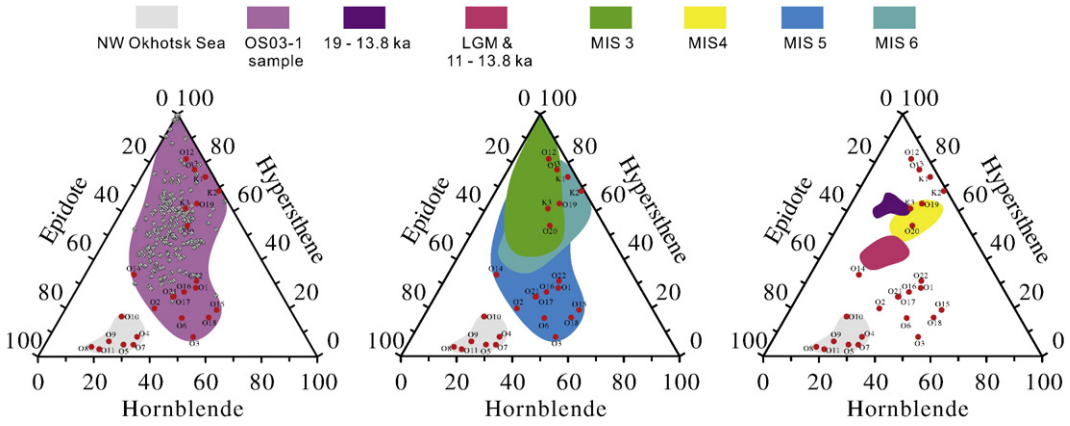

Fig. 5. Ternary plot of hornblende-epidote-hypersthene showing provenance of heavy minerals investigated from core OS03-1.The numbers O1, O2, K1, K2, and so on, correspond different heavy mineral provenances mentioned in Fig. 1.

that the provenance of coarse fractions may vary between cold and warm periods. The coarse fraction mainly sourced from the eastern shelf and the western area of the Kamchatka Peninsula during cold periods (MIS 6, MIS 4 and MIS 2). Nürnberg et al. (2011) proposed that the IRD composition of late MIS 6 in core LV28-44-3 located at the western Kamchatka Peninsula, mainly originated from Sredinny Mountain Range of Kamchatka. Based on magnetic mineral grains, Chou et al. (2011) inferred that the coarse fractions derived from the Kamchatka Peninsula by river ice erosion in cold glacial periods were brought to the central Okhotsk Sea (MD01-2414) by the western Kamchatka Current. Our data strongly support such an idea and further attested that the eastern Kamchatka Peninsula also contributed to the sediment composition in the southern Okhotsk Sea. Evidence also exists that glaciers transport IRD and drop-stones into the Pacific Ocean from the eastern part of the Kamchatka Peninsula (Bigg et al., 2008). During MIS 5, the provenance of coarse fraction extended from the eastern Okhotsk Sea to the northern and northeast shelf of Okhotsk Sea (Fig. 5). In comparison, the provenance of sediments accumulated during MIS 3 and 6 was almost similar (Fig. 5), except for volcanic materials.

The forms and lithology of drop-stones in core OS03-1 also revealed the signs of ice rafting sources. Large drop-stones may have four possible sources: (1) the Sakhalin Island offshore ice rafted deposits or the Amur River input; (2) the coastal sediments of the northwest and the north shelves; (3) the icebergs derived from the Kamchatka Peninsula; and (4) volcanic eruption from the Kamchatka Peninsula or the Kuril Islands. By comparing rock properties on the east coast of Sakhalin and sediment inputs from the Amur River, the first possibility is eliminated. Coarse sand content was the highest (on average > 10%) in surface sediments on the northern coast of Sakhalin Island, whereas coarse grain content was 1.5%–7.6% on the east coast of island (Sakamoto et al., 2005). The Amur River input material is mainly deposited in the eastern part of the island. The second and third sources show correlations with the sea ice transportation and expansion. The drop-stones with petrology forms which are mainly dacite, andesite and rhyolite in core OS03-1 are similar with the lithology of the outcrop in the northern shelf of Okhotsk Sea, which mainly contains dacite and rhyolite (Tikhomirov et al., 2012). According to the lithology, shape and size of the drop-stones, we can easily remove the fourth. According to the descriptions of different deposition agents and the characteristics of drop-stones (Bennett et al., 1994), the drop-stones in core OS03-1 should be carried by sea ice and derived from the northeast shelves and east of the Okhotsk Sea.

The variation in sediment sources in core OS03-1 over the last 180 ka is also recorded by various volcanic detritus. Volcanic detritus is widespread in the Okhotsk Sea and is mainly from the neighbouring volcanic belts, such as Kamchatka Peninsula, Kuril Islands, and Sakhalin Islands. The clay mineral assemblage is characterized by high content but significant spatial variation of montmorillonite, an indicator of volcanic detritus, in the surface sediments of the Okhotsk Sea (Aoki and Oinuma, 1978), attested the contribution from the volcanic detritus to the sediment composition.

For K2 tephra that originates the eruption of the Nemo Volcano, Nemo-IIIcaldera, located in the Onekotan Island, the transparent glass content is 9.37% (average content) while the content is 0.16% for brown glass in the OS03-1. KO tephra is a very important Early Holocene marker for the southern part of Kamchatka. The tephra is a mixture of yellowish, fine to coarse ash. Mineral assemblage comprises by volcanic glass, plagioclase, pyroxene and magnetite. Volcanic glass dominates in tephra (Braitseva et al., 1997). In the lower part of core OS03-1 (MIS 6), the contents of brown volcanic glass and cinder are high, whereas in the upper section (MIS 5 and 3), the content of transparent volcanic glass exhibited a similar trend with high values. Volcanic glass of various colors in the core suggests different provenances. If the coarse fraction provenance deduction derived from heavy minerals is correct, then it is reasonable that the brown volcanic glass in the lower core was most likely from the Kamchatka Peninsula, while during MIS 5 and MIS 3, increasing content of transparent volcanic glass was mainly from the Kuril Islands.

5.3. Cause of provenance changes in the Okhotsk Sea

Based on changes in the heavy mineral assemblages, we have defined several provenance changes throughout the studied core. The mineral supply of coarse fraction is mainly decided by sea ice transport, forced by winds and ocean currents (Leppäranta, 2011). Modern observations of sea ice and sea level pressures show that the seasonal sea ice growth for the Okhotsk Sea and the Bering Sea is associated with the positions of the Aleutian Low (Cavalieri and Parkinson, 1987). This atmospheric system is the main agent that transports sea ice with entrained sediment material from the northeast and east margins into the Okhotsk Sea (Fig. 6).

The inferred provenance changes with various heavy mineral assemblages in core OS03-1 during warm and cold periods, indicating the changes of winds and ocean circulations in the past. The major contribution from the western Kamchatka Peninsula suggests that the easterly wind was dominant during cold periods (MIS 6, 4, 3), while the northward shift from the western Kamchatka Peninsula to the northeast margins in the Okhotsk Sea indicates that northeasterly wind was dominant during MIS 5 (Fig. 6). This change in wind direction between warm and cold periods indicates the variation of atmospheric patterns over the Okhotsk Sea. In accordance with the abundance of radiolarian *C. davisiana* in sediment cores collected from the southwest Okhotsk Sea, Itaki and Ikehara (2004) proposed that the central position of Aleutian Low shifted south from early Holocene to late Holocene,

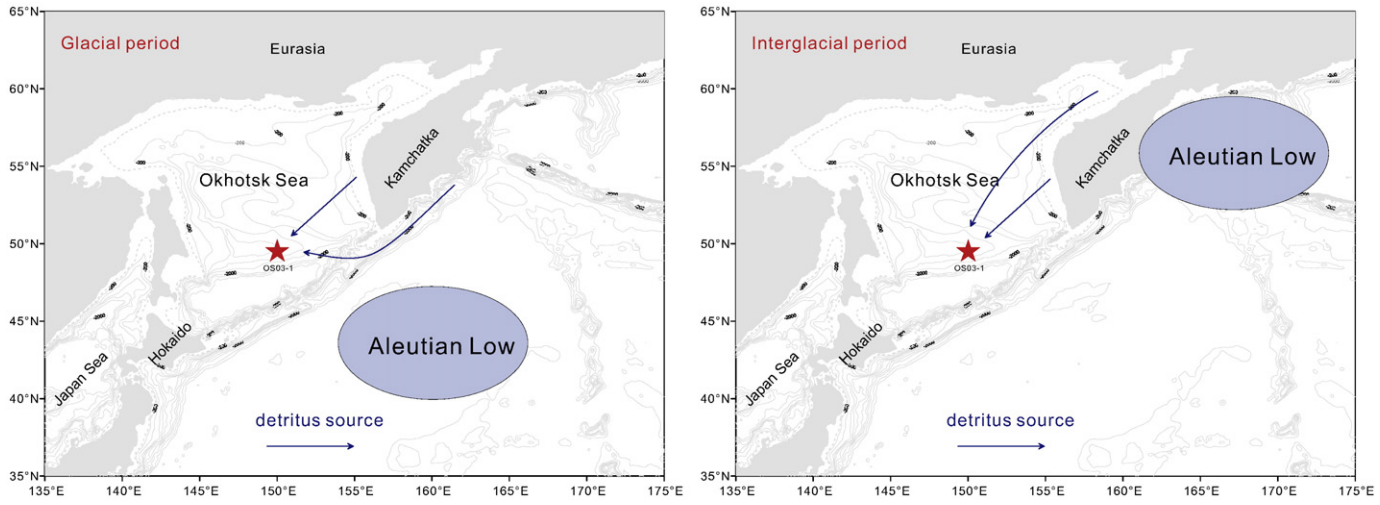

Fig. 6. A schematic illustration depicts the sediment provenance and the atmospheric pressure patterns over the Okhotsk Sea in the glacial and interglacial periods.

accompanied by an enhanced sea ice cover. Later, Katsuki et al. (2010) extended the time slice into the Last Glacial Maximum for the relationship between sea ice distribution and atmospheric pressure patterns using the relative abundance of the sea ice diatom species. The provenance discrimination diagram reveals the contribution from the western Kamchatka Peninsula, which indicated the southern location of the Aleutian Low during cold periods (MIS 6 and 4). Similarly, our heavy minerals data also supported different provenances during the Last Glacial Maximum and the last deglacial period (Fig. 5). Katsuki et al. (2010) assumed that the south Aleutian Low and strong Siberian High were dominant before 15 ka and during 15–10 ka, respectively, which could explain the provenance difference in these two time intervals (Fig. 5). During MIS 5, besides the areas around the Kamchatka Peninsula, other provenances include the north and northeast shelves of the Okhotsk Sea and enhanced terrigenous supply suggests larger source areas of sea ice at our core site. In general, the dominant easterly wind that shifts to northeasterly during cold periods (MIS 6 and 4) to warm period (MIS 5) due to the northward shift of the Aleutian Low.

On the other hand, discriminant diagram of provenance (Fig. 5) suggests the transportation of terrigenous material from the eastern Kamchatka Peninsula to the core site. The modern mountain glaciers calve from the east of the Kamchatka peninsula (Sakamoto et al., 2005). The contents of both IP_{25} (highly branched isoprenoid sea ice biomarker) and diatom species (sea ice and open water) in core SO201-2-12 located at the East Kamchatka Peninsula (Fig. 1) suggest a resembled seasonal sea ice coverage between H1 and YD (Méheust et al., 2016; Max et al., 2012). Therefore, it is reasonable to speculate that detrital materials entrained in sea ice on east Kamchatka Peninsula most probably is transported to the southern Okhotsk Sea by the Kamchatka Current during MIS 6. Previous reports suggest that the source of most of the terrigenous material is from the Kamchatka glacier sheet (Nürnberg et al., 2011; Sakamoto et al., 2005). However, the problem with this assumption is that the western edge of mountain glaciers on the Kamchatka Peninsula is almost 1500 m above the sea level. In addition, Meyer et al. (2016) reported that MAT-derived summer SST in east Kamchatka during the Last Glacial Maximum (LGM) was as high as present. If so, then the extent of sea ice in the east Kamchatka Peninsula was limited at this time. The variations in the Kamchatka Current and its role in the transport of detrital sediment deserve further investigation.

5.4. Sea ice history in the Okhotsk Sea

The increase in IRD content in the cores is directly related to the expansion of sea ice under colder climatic conditions (Sakamoto et al., 2005). During the LGM, perennial sea ice cover could not have occurred in the Okhotsk Sea (Shiga and Koizumi, 2000). The accumulation rates of dominant light and heavy minerals (quartz, plagioclase, hornblende, epidote) in core OS03-1 show similar trends with increasing IRD fluxes in MIS 6,Termination II, MIS 5.3, MIS 4 and LGM, which corresponds with low or decreasing SST in cores MD01-2412 and ODP 885 (Fig. 6). In order to get insights into a full picture of sea ice change, we compare the record of core OS03-1 with other cores, as presented in Fig. 1.

5.4.1. MIS 6

Previous reports have suggested that heavy glaciation existed during MIS 6 in the Okhotsk Sea (Nürnberg et al., 2011; Wang and Wang, 2008). The typical characteristics for the average quartz fluxes in core OS03-1 was a factor of 3–5 higher during early MIS 6, as compared to that of the LGM. Similar scenario but with higher quartz fluxes also occurred in the central Okhotsk Sea (core LV28-41-4) (Nürnberg et al., 2011). A possible reason is that the location of core OS03-1 is much closer to the open subarctic Pacific. Because of the IRD fluxes from the East-West section, Nürnberg et al. (2011) concluded that the depositional centre has shifted from the west Okhotsk Sea (early MIS 6) toward Kamchatka (late MIS 6), suggesting a change in sediment provenance. High siliciclastic fluxes in cores MD01–2415 and LV28-42-5 did not exist during the early MIS 6 (Nürnberg et al., 2011; Nürnberg and Tiedemann, 2004), but occurred in ODP 145-882 in the subarctic North Pacific (Haug, 1995). Synchronous enhanced accumulation rates of detrital materials in cores OS03-1 and ODP 145-882 suggest that areas around the eastern Kamchatka Peninsula might have contributed to the terrigenous deposition during MIS 6. Prevailing sestonophagous species of benthic foraminifera in core LV28-44-3 characterized a dynamic and intense production of the Okhotsk Sea Intermediate Water in glacial periods (Khusid et al., 2005). Therefore, we suggest that the extent and duration of sea ice in the northern and eastern Okhotsk Sea might have expanded in MIS 6.

5.4.2. MIS5

The IRD accumulation rate in MIS5 is relatively low, but two peaks of IRD flux occurred in Termination II (MIS6/5) (slight) and MIS 5.3 (high), indicating a seasonal sea ice condition at site OS03-1. Provenance analysis shows that the detritus materials mainly come from the northern and western Okhotsk Sea during MIS 5, indicating a scenario with decreasing seasonal sea ice cover or ice-free condition at the core site and prevailing northeasterly winds. In Termination II, high IRD fluxes occurred in the eastern and central Okhotsk Sea, but not in the western subarctic Pacific (ODP145-882). The high IRD flux during MIS5.3 is noteworthy. Zou et al. (2015) reported high accumulation rates of rare earth elements and suggested that they corresponded to an intensified

Siberian High Index in MIS 5.3 (Li and Liu, 2012). The ratio of hypersthene to hornblende shows an increased volcanic detritus contribution in MIS 5.3. We also noticed that opal content was even higher in MIS 5.3 than that in MIS 5.5 in ODP 145-885 (Jaccard et al., 2009). A potential linkage maybe existed between these two sites. We assume that an increased sea ice formation synchronously improves the IRD accumulation rate in core OS03-1 and diatom blooming in the western subarctic Pacific in MIS 5.3. For other intervals, especially in MIS 5.5, low IRD accumulation rates suggest that seasonal sea ice gave way to ice-free conditions with sporadic ice transported in winter. High $CaCO_3$ contents together with abundances of diatom and foraminifera (Barash et al., 2005; Khusid et al., 2005; Wang and Wang, 2008) support this finding.

5.4.3. MIS 4 & LGM

Low abundances of diatom, benthic foraminifera and decreased productivity in the central and western Okhotsk indicated a heavily expanded sea ice condition. Shiga and Koizumi (2000) studied diatoms in several cores of the Okhotsk Sea and showed that permanent ice only existed in the western part of the Okhotsk Sea during MIS 2. Radiolarian data also showed similar results near the Sakhalin Island Core XP98-PC4 (Fig. 1) in MIS 2 when seasonal sea ice existed in the area (Okazaki et al., 2003a, 2003b). In core OS03-1, a slightly increased IRD flux indicates an expanded seasonal sea ice cover in the southern Okhotsk Sea. High terrigenous biomarkers in core GGC-15 (Ternois et al., 2001) next to our core OS03-1, supported an increased terrigenous inputs during the Last Glacial Period. IRD records in cores from the eastern to southwestern Okhotsk Sea all show an expanded sea ice coverage in the LGM and MIS 4 and had seasonal sea ice conditions in MIS 4 and 2 (Sakamoto et al., 2006).

5.4.4. MIS 3

Similar sediment provenance in MIS 6 and MIS 3 in core OS03-1 suggests a comparable condition of sea ice transportation. Comparing the IRD flux record of OS03-1 with that of core LV28-44-3 from the eastern Okhotsk Sea (Fig. 7), we found that both records show similar trends in the early MIS 3 (41–59 ka) but different patterns in the late MIS 3. Bigg et al. (2008) postulated that the Kamchatka Ice Sheet occurred during the last glacial period and ended after 14 ka. Nürnberg et al. (2011) reported a high IRD flux, quasi millennial-scale variation in the eastern Okhotsk Sea (LV28-44-3) in the late MIS 3 (Fig. 7) and proposed that high flux was attributed to iceberg supply from the Kamchatka. High siliciclastic flux also presented in ODP 145-882 in MIS3 (Haug, 1995). However, there are no high IRD fluxes in OS03-1 and other sediment

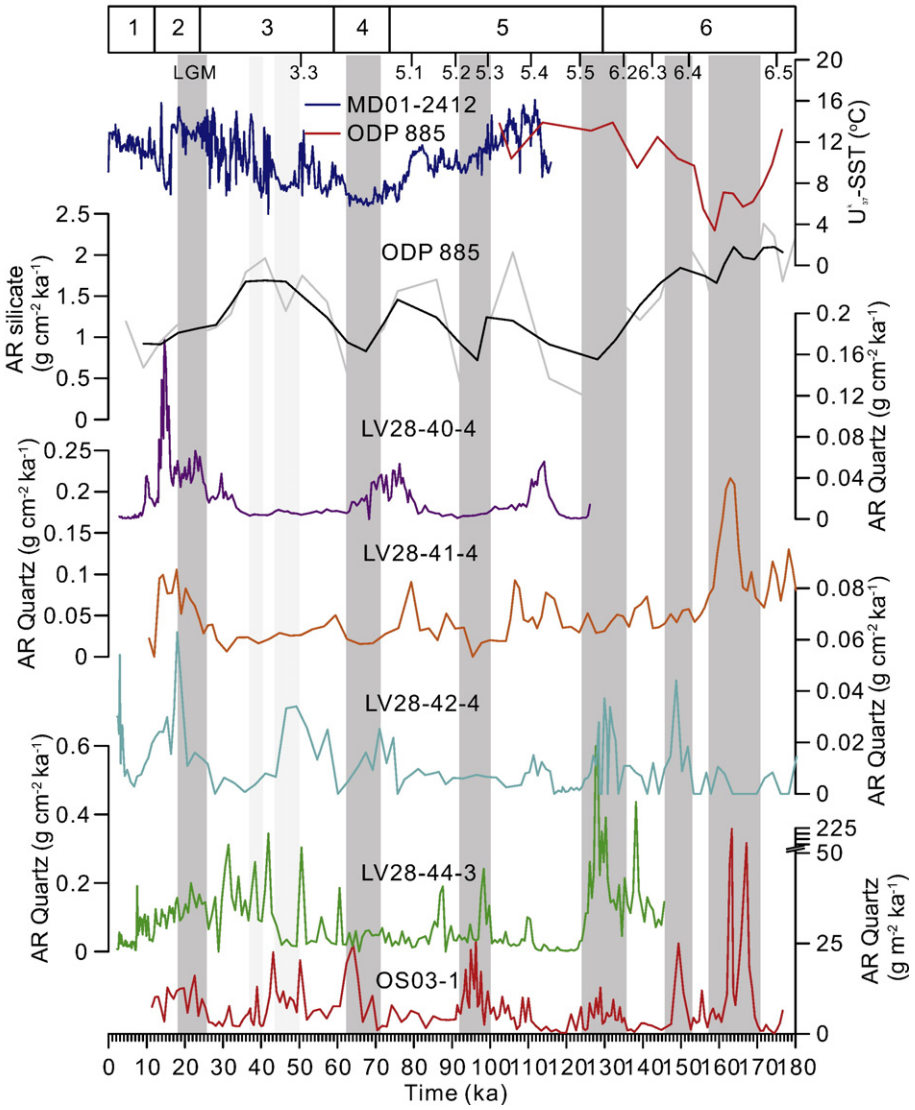

Fig. 7. Down core profiles of accumulation rate of quartz in fraction of 63–125 μm in core OS03-1 compared with other records of accumulation rate of quartz in cores LV28-40-4, LV28-41-4, LV28-42-4 and LV28-44-4 along the west-east section (Nürnberg et al., 2011) in the Okhotsk Sea and U^{k}_{37}-derived SST in cores MD01-2412 (Harada et al., 2008) and ODP145-882 (Martínez-Garcia et al., 2010). Note: the quartz contents in Nürnberg et al. (2011) were identified from the size class 125–500 μm.

cores located at the central and western Okhotsk Sea. Therefore we speculate that a long interval of seasonal sea ice cover existed in the Okhotsk Sea during the late MIS3 (Fig. 7).

6. Conclusions

The records of light and heavy minerals in core OS03-1 provided insight into sediment provenance, sea ice transportation, and past climate changes in the southern Okhotsk Sea over the past 180 ka BP. Sea ice was the main agent for the transportation of terrigenous materials from the land to ocean. The representative terrigenous minerals are plagioclase, quartz, hornblende, augite, epidote and garnet. The volcanic minerals found in the studied core are hypersthene, magnetite and volcanic glass. The provenance change from the eastern Okhotsk Sea during glacial intervals to the north and northeastern Okhotsk Sea during interglacial intervals correlates to the varied position of Aleutian Low in different time slices. The detritus input was high during glacial periods and low during interglacial periods, indicating an expanded and decreased seasonal sea ice cover in the Okhotsk Sea respectively.

Acknowledgements

We are very grateful to editor and two anonymous reviewers for their critical reviews and suggestions that helped us to further improve this paper and thank Dr. A. A. Bosin for providing references in mineralogy. Financial support was provided by the International Cooperation Project of Global Change and Ocean-Atmosphere Interaction (GASI-GEOGE-04) and National Natural Science Foundation of China (Grant Nos.:40706030, 41476056, 41611130042, 41206059 and U1606401) and by the Basic Scientific Fund for National Public Research Institutes of China (No. 2007T09 and 2016Q09) and by the AoShan Talents Program Supported by Qingdao National Laboratory for Marine Science and Technology (No. 2015ASTP-ES16) and Taishan Scholarship from Shandong Province and International Cooperative Projects in polar regions (201613).

Appendix A. Supplementary data

Supplementary data to this article can be found online at http://dx.doi.org/10.1016/j.palaeo.2017.04.017.

References

Aoki, S., Oinuma, K., 1978. The distribution of clay minerals in recent sediments of the Okhotsk Sea. Deep-Sea Res. 25, 659–667.
Barash, M.S., Chekhovskaya, M.P., Biebow, N., Nurnberg, D., Tiedeman, R., 2005. About Quaternary paleoceanography in the southeast part of the Okhotsk Sea, from lithology and planktic foraminifera. Okeanologiya 45, 273–285.
Bennett, M.R., Doyle, P., Matherf, A.E., Woodfin, J.L., 1994. Testing the climatic significance of dropstones: an example from southeast Spain. Geol. Mag. 131, 845–848.
Bigg, G.R., Clark, C.D., Hughes, A.L.C., 2008. A last glacial ice sheet on the Pacific Russian coast and catastrophic change arising from coupled ice–volcanic interaction. Earth Planet. Sci. Lett. 265, 559–570.
Bischof, J., Clark, D.L., Vincent, J.-S., 1996. Origin of ice-rafted debris: Pleistocene paleoceanography in the western Arctic Ocean. Paleoceanography 11, 743.
Braitseva, O.A., Ponomareva, V.V., Sulerzhitsky, L.D., Melekestsev, I.V., Bailey, J., 1997. Holocene key-marker tephra layers in Kamchatka, Russia. Quat. Res. 47, 125–139.
Carter, L., Neil, H.L., Northcote, L., 2002. Late Quaternary ice-rafting events in the SW Pacific Ocean, of eastern New Zealand. Mar. Geol. 191, 19–35.
Cavalieri, D.J., Parkinson, C.L., 1987. On the relationship between atmospheric circulation and the fluctuations in the sea ice extents of the Bering and Okhotsk seas. J. Geophys. Res. Oceans 92, 7141–7162.
Chou, Y.-M., Lee, T.-Q., Song, S.-R., Chen, K.-J., 2011. Magnetostratigraphy of marine sediment core MD01-2414 from Okhotsk Sea and its paleoenvironmental implications. Mar. Geol. 284, 149–157.
Derkachev, A.N., Nikolaeva, N.A., 2007. Chapter 17 multivariate analysis of heavy mineral assemblages of sediments from the marginal seas of the Western Pacific. In: Maria, A.M., David, T.W. (Eds.), Developments in Sedimentology. Elsevier, pp. 439–464.
Derkachev, A.N., Nikolaeva, N.A., Gorbarenko, S.A., Harada, N., Sakamoto, T., Iijima, K., Sakhno, V.G., Hua Hua, L., Wang, K., 2012. Characteristics and ages of tephra layers in the central Okhotsk Sea over the last 350 kyr. Deep-Sea Res. II Top. Stud. Oceanogr. 61–64, 179–192.
Dowdeswell, J.A., 2009. Ice-rafted debris (IRD). In: Gornitz, V. (Ed.), Encyclopedia of Paleoclimatology and Ancient Environments. Springer, pp. 471–473.
Gorbarenko, S.A., Khusid, T.A., Basov, I.A., Oba, T., Southon, J.R., Koizumi, I., 2002. Glacial Holocene environment of the southeastern Okhotsk Sea: evidence from geochemical and palaeontological data. Palaeogeogr. Palaeoclimatol. Palaeoecol. 177, 237–263.
Gorbarenko, S.A., Harada, N., Malakhov, M.I., Vasilenko, Y.P., Bosin, A.A., Gol'dberg, E.L., 2008. Millennial-scale climatic and environmental oscillations in the Sea of Okhotsk in response to global changes during the last 190 ka. Dokl. Earth Sci. 423, 1410–1413.
Harada, N., Sato, M., Sakamoto, T., 2008. Freshwater impacts recorded in tetraunsaturated alkenones and alkenone sea surface temperatures from the Okhotsk Sea across millennial-scale cycles. Paleoceanography 23.
Haug, G., 1995. Paleoceanography and Sedimentation History in the Pacific Northwest During the Last 6 Million Years (ODP Site 882). University of Kiel, Kiel, pp. 1–142.
Itaki, T., Ikehara, K., 2004. Middle to late Holocene changes of the Okhotsk Sea Intermediate Water and their relation to atmospheric circulation. Geophys. Res. Lett. 31.
Jaccard, S.L., Galbraith, E.D., Sigman, D.M., Haug, G.H., Francois, R., Pedersen, T.F., Dulski, P., Thierstein, H.R., 2009. Subarctic Pacific evidence for a glacial deepening of the oceanic respired carbon pool. Earth Planet. Sci. Lett. 277, 156–165.
John, K.E.K.S., Krissek, L.A., 1999. Regional patterns of Pleistocene ice-rafted debris flux in the North Pacific. Paleoceanography 14, 653.
Katsuki, K., Khim, B.-K., Itaki, T., Okazaki, Y., Ikehara, K., Shin, Y., Yoon, H.I., Kang, C.Y., 2010. Sea-ice distribution and atmospheric pressure patterns in southwestern Okhotsk Sea since the Last Glacial Maximum. Glob. Planet. Chang. 72, 99–107.
Khusid, T.A., Barash, M.S., Biebow, N., Nurnberg, D., Tiedemann, R., 2005. Late quaternary environmental changes on the southeastern slope of the Sea of Okhotsk inferred from benthic foraminifera. Oceanology 45, 413–419.
Kimura, N., Wakatsuchi, M., 1999. Processes controlling the advance and retreat of sea ice in the Sea of Okhotsk. J. Geophys. Res. Oceans 104, 11137–11150.
Leppäranta, M., 2011. The Drift of Sea Ice. Springer Science & Business Media.
Li, X., Liu, X., 2012. A transient simulation of East Asian paleoclimate changes in response to insolation forcing during the past 150 ka. J. Earth Environ. 3, 805–812 (in Chinese with English abstract).
Liu, Y.-J., Song, S.-R., Lee, T.-Q., Lee, M.-Y., Chen, Y.-L., Chen, H.-F., 2006. Mineralogical and geochemical changes in the sediments of the Okhotsk Sea during deglacial periods in the past 500 kyrs. Glob. Planet. Chang. 53, 47–57.
Malakhov, M.I., Gorbarenko, S.A., Malakhova, G.Y., Harada, N., Vasilenko, Y.P., Bosin, A.A., Gol'dberg, E.L., Derkachev, A.N., 2009. Petromagnetic parameters of bottom sediments as indicators of the climatic and environmental changes in the central zone of the Sea of Okhotsk during the last 350 kyr. Russ. Geol. Geophys. 50, 973–982.
Martin, S., Drucker, R., Yamashita, K., 1998. The production of ice and dense shelf water in the Okhotsk Sea polynyas. J. Geophys. Res. 103, 27771–27782.
Martínez-Garcia, A., Rosell-Melé, A., McClymont, E.L., Gersonde, R., Haug, G.H., 2010. Subpolar link to the emergence of the modern Equatorial Pacific cold tongue. Science 328, 1550–1553.
Max, L., Riethdorf, J.-R., Tiedemann, R., Smirnova, M., Lembke-Jene, L., Fahl, K., Nürnberg, D., Matul, A., Mollenhauer, G., 2012. Sea surface temperature variability and sea-ice extent in the subarctic northwest Pacific during the past 15,000 years. Paleoceanography 27. http://dx.doi.org/10.1029/2012PA002292.
Méheust, M., Stein, R., Fahl, K., Max, L., Riethdorf, J.-R., 2016. High-resolution IP25-based reconstruction of sea-ice variability in the western North Pacific and Bering Sea during the past 18,000 years. Geo-Mar. Lett. 36, 101–111.
Meyer, V.D., Hefter, J., Lohmann, G., Tiedemann, R., Mollenhauer, G., 2016. Summer-temperature evolution on the Kamchatka Peninsula, Russian Far East, during the past 20,000 years. Clim. Past Discuss. http://dx.doi.org/10.5194/cp-2016-21 (in review).
Minervin, I.G., Romanyuk, V.A.E., Pishchal'nik, V.M., Truskov, P.A.E., Pokrashenko, S.A., 2015. Zoning the ice cover of the Sea of Okhotsk and the Sea of Japan. Her. Russ. Acad. Sci. 85, 132–139.
Nicholson, U., Poynter, S., Clift, P.D., Macdonald, D.I.M., 2014. Tying catchment to basin in a giant sediment routing system: a source-to-sink study of the Neogene–recent Amur River and its delta in the North Sakhalin Basin. Geol. Soc. Lond., Spec. Publ. 386, 163–193.
Nürnberg, D., Tiedemann, R., 2004. Environmental change in the Sea of Okhotsk during the last 1.1 million years. Paleoceanography 19:PA4011. http://dx.doi.org/10.1029/2004PA001023.
Nürnberg, D., Wollenburg, I., Dethleff, D., Eicken, H., Kassens, H., Letzig, T., Reimnitz, E., Thiede, J., 1994. Sediments in Arctic sea ice: implications for entrainment, transport and release. Mar. Geol. 119, 185–214.
Nürnberg, D., Dethleff, D., Tiedemann, R., Kaiser, A., Gorbarenko, S.A., 2011. Okhotsk Sea ice coverage and Kamchatka glaciation over the last 350 ka — evidence from ice-rafted debris and planktonic $\delta^{18}O$. Palaeogeogr. Palaeoclimatol. Palaeoecol. 310, 191–205.
Ogi, M., Tachibana, Y., Nishio, F., Danchenkov, M.a., 2001. Does the fresh water supply from the Amur River flowing into the Sea of Okhotsk affect sea ice formation? J. Meteorol. Soc. Jpn. 79, 123–129.
Okazaki, Y., Takahashi, K., Yoshitani, H., Nakatsuka, T., Ikehara, M., Wakatsuchi, M., 2003a. Radiolarians under the seasonally sea-ice covered conditions in the Okhotsk Sea: flux and their implications for paleoceanography. Mar. Micropaleontol. 49, 195–230.
Okazaki, Y., Takahashi, K., Nakatsuka, T., Honda, M.C., 2003b. The production scheme of *Cycladophora davisiana* (Radiolaria) in the Okhotsk Sea and the northwestern North Pacific: implication for the paleoceanographic conditions during the glacials in the high latitude oceans. Geophys. Res. Lett. 30, 1939.
Okazaki, Y., Takahashi, K., Katsuki, K., Ono, A., Hori, J., Sakamoto, T., Uchida, M., Shibata, Y., Ikehara, M., Aoki, K., 2005. Late Quaternary paleoceanographic changes in the southwestern Okhotsk Sea: evidence from geochemical, radiolarian, and diatom records. Deep-Sea Res. II Top. Stud. Oceanogr. 52, 2332–2350.

Petelin, V.P., 1957. Mineralogy of sandy-silt sediment fractions of the Sea of Okhotsk. Proceedings of the Oceanological Institute of the USSR Academy of Sciences (in Russian). 22, pp. 77–138.
Qiu, B., 2001. Kuroshio and Oyashio currents. In: John, H.S., Karl, K.T., Steve, A.T. (Eds.), Encyclopedia of Ocean Sciences, second ed. Academic Press, Oxford, pp. 358–369.
Sakamoto, T., Ikehara, M., Aoki, K., Iijima, K., Kimura, N., Nakatsuka, T., Wakatsuchi, M., 2005. Ice-rafted debris (IRD)-based sea-ice expansion events during the past 100 kyrs in the Okhotsk Sea. Deep-Sea Res. II Top. Stud. Oceanogr. 52, 2275–2301.
Sakamoto, T., Ikehara, M., Uchida, M., Aoki, K., Shibata, Y., Kanamatsu, T., Harada, N., Iijima, K., Katsuki, K., Asahi, H., Takahashi, K., Sakai, H., Kawahata, H., 2006. Millennial-scale variations of sea-ice expansion in the southwestern part of the Okhotsk Sea during the past 120 kyr: age model and ice-rafted debris in IMAGES Core MD01-2412. Glob. Planet. Chang. 53, 58–77.
Selvaraj, K., Chen, C.-T.A., Babu, C.P., Lou, J.-Y., Liu, C.-L., Hsu, K.J., 2012. Glacially derived material in an Inner Mongolian desert lake during Marine Isotope Stage 2. J. Quat. Sci. 27, 725–733.
Shiga, K., Koizumi, I., 2000. Latest Quaternary oceanographic changes in the Okhotsk Sea based on diatom records. Mar. Micropaleontol. 38, 91–117.
Simizu, D., Ohshima, K.I., Ono, J., Fukamachi, Y., Mizuta, G., 2014. What drives the southward drift of sea ice in the Sea of Okhotsk? Prog. Oceanogr. 126, 33–43.
Small, D., Parrish, R.R., Austin, W.E.N., Cawood, P.a., Rinterknecht, V., 2013. Provenance of North Atlantic ice-rafted debris during the last deglaciation-a new application of U-Pb rutile and zircon geochronology. Geology 41, 155–158.
Takahashi, K., 1998. The Bering and Okhotsk seas: modern and past paleoceanographic changes and gateway impact. J. Asian Earth Sci. 16, 49–58.
Ternois, Y., Kawamura, K., Keigwin, L., Ohkouchi, N., Nakatsuka, T., 2001. A biomarker approach for assessing marine and terrigenous inputs to the sediments of Sea of Okhotsk for the last 27,000 years. Geochim. Cosmochim. Acta 65, 791–802.
Tikhomirov, P.L., Kalinina, E.A., Moriguti, T., Makishima, A., Kobayashi, K., Cherepanova, I.Y., Nakamura, E., 2012. The Cretaceous Okhotsk–Chukotka Volcanic Belt (NE Russia): geology, geochronology, magma output rates, and implications on the genesis of silicic LIPs. J. Volcanol. Geotherm. Res. 221–222, 14–32.
Untersteiner, N., 1986. The geophysics of sea ice: overview. In: Untersteiner, N. (Ed.), The Geophysics of Sea Ice. Springer US, Boston, MA, pp. 1–8.
Wang, W.-L., Wang, L.-C., 2008. Reconstruction of oceanographic changes based on the diatom records of the central Okhotsk Sea over the last 500000 years. Terr. Atmos. Ocean. Sci. 19, 403–411.
Wang, K., Shi, X., Wu, Y., Zou, J., Jiang, X., 2014. Characteristics and provenance imolications of heavy mineral in core OS03-1 from the east-southern Okhotsk Sea. Acta Oceanol. Sin. 36, 177–185 (in Chinese).
Yang, J., Honjo, S., 1996. Modeling the near-freezing dichothermal layer in the Sea of Okhotsk and its interannual variations. J. Geophys. Res. 101, 16421.
Yasuda, T., Asahara, Y., Ichikawa, R., Nakatsuka, T., Minami, H., Nagao, S., 2014. Distribution and transport processes of lithogenic material from the Amur River revealed by the Sr and Nd isotope ratios of sediments from the Sea of Okhotsk. Prog. Oceanogr. 126, 155–167.
Zhabin, I.A., Abrosimova, A.A., Dubina, V.A., Nekrasov, D.A., 2010. Influence of the Amur River runoff on the hydrological conditions of the Amur Liman and Sakhalin Bay (Sea of Okhotsk) during the spring-summer flood. Russ. Meteorol. Hydrol. 35, 295–300.
Zou, J., Shi, X., Zhu, A., Chen, M.-T., Kao, S., Wu, Y., Selvaraj, K., Scholz, P., Bai, Y., Wang, K., Ge, S., 2015. Evidence of sea ice-driven terrigenous detritus accumulation and deep ventilation changes in the southern Okhotsk Sea during the last 180 ka. J. Asian Earth Sci. 114, 541–548.